Available online at www.sciencedirect.com
SCIENCE DIRECT®
Journal of Nuclear Materials 335 (2004) 493–500
journal of nuclear materials
www.elsevier.com/locate/jnucmat

Desorption of water adsorbed on iron oxide by laser irradiation

K. Chiba, S. Tanaka *, T. Yoneoka

Department of Quantum Engineering and System Science, The University of Tokyo, 7-3-1 Hongo Bunkyo-ku, Tokyo 113-8656, Japan

Received 23 June 2003; accepted 6 September 2004

Abstract

Desorption of water adsorbed on iron oxide by laser irradiation was studied by means of a time-of-flight (TOF) technique. The wavelength of the laser for desorption was varied from 355 to 600 nm. The energy threshold of the water desorption ranged around 2.0–2.3 eV. Based on the fact that this energy threshold approximately corresponds to the bandgap of Fe_2O_3, the initial process of water desorption is considered to be the electronic excitation of the iron oxide from the valence band to the conduction band. Analysis of the velocity distribution of the desorbed water suggests that following the electronic excitation of the iron oxide the desorption is caused by both thermal and nonthermal processes. The thermal process is caused by the rise of the surface temperature that occurs after the scattering and de-excitation of the excited electron in the iron oxide. In the case of the laser at $\lambda = 355$ nm, the desorption was mainly caused by the thermal process. On the other hand, in the case of the laser at $\lambda = 430$ nm, the desorption was mainly caused by the nonthermal process. The desorption caused by the nonthermal process is attributed to the transfer of the electron excited in the iron oxide to the adsorbed hydroxyl.

PACS: 28.52.Nh

1. Introduction

From the viewpoint of tritium safety in a fusion reactor, an effective method for tritium decontamination is needed [1–7]. Irradiation of energetic particles (electrons, photons, or ions) on the surface of various component materials of a fusion reactor is considered one method of tritium decontamination [3–7]. The desorption mechanism of species adsorbed on the surface by the irradiation of energetic particles has been investigated in various systems [3–17]. Before applying the method of irradiation of energetic particles to tritium decontamination, it is important to elucidate the basic desorption mechanism and to evaluate the decontamination efficiency in actual conditions. In our previous studies [4–7], we conducted a mass analysis of desorbed species using a Hg–Xe lamp and a deuterium lamp as a photon source and a quadruple mass spectrometer (QMS) for analyzing the desorbed species, and our findings suggested that the desorption of water from the surface of the iron oxide was caused not only by the thermal process via the rise of the surface

* Corresponding author. Tel.: +81 3 5841 6968; fax: +81 3 5841 8625.
E-mail address: s-tanaka@q.t.u-tokyo.ac.jp (S. Tanaka).

0022-3115/$ - see front matter © 2004 Elsevier B.V. All rights reserved.
doi:10.1016/j.jnucmat.2004.09.001

temperature but also by the nonthermal process that followed electron transfer from the iron oxide to the adsorbed hydroxyl. However, the desorption mechanism was not elucidated in detail. In order to elucidate the desorption mechanism by photon irradiation, it is necessary to analyze the velocity distribution of the desorbed species and the dependence of desorption behavior on the photon energy. This is because the velocity distribution and the dependence of desorption behavior on the photon energy give important information about the desorption mechanism. In the present study, in order to obtain the velocity distribution of the desorbed species by photon irradiation, a time-of-flight (TOF) technique was used.

The surface of metallic materials in actual conditions is often covered with an oxide film or organic matter. In the present study, we used H_2O or D_2O as a simulant of HTO and an iron covered with a thin film of iron oxide as one of the metallic materials.

2. Experimental

Desorption experiments were carried out in a vacuum chamber for TOF analysis. Fig. 1 shows the experimental apparatus used for these experiments. The apparatus is equipped with a micro-channel plate (MCP) to detect the desorbed species, a quadruple mass spectrometer (QMS), and a fused quartz window for introduction of the lasers into the chamber. A tunable laser (HOYA CONTINUUM CORPORATION, Panther OPO, pulse duration = 3–5 ns) pumped by a third harmonic (355 nm) of a Nd:YAG laser (HOYA CONTINUUM CORPORATION Surlite II-10, pulse duration = 4–6 ns) irradiated the sample surface at 45° from the sample normal via the fused quartz window for desorption of water adsorbed on the sample surface. The wavelength of the laser can be tuned from 430 to 700 nm using an optical parametric oscillator (OPO) system. The typical laser spot on the surface was about 0.3 cm^2. The laser shot repetition was 10 Hz. In order to detect the desorbed species using the MCP, a fourth harmonic (266 nm) of a Nd:YAG laser (HOYA CONTINUUM CORPORATION, Surlite I-10, pulse duration = 4–6 ns) was used to ionize the desorbed species after the laser irradiation for desorption. The laser power for ionization was about 40 mJ/pulse and the diameter 6 mm. The laser for ionization was focused by a quartz lens with a focal length of 300 mm. The diameter of the laser at the focal point was estimated to be about 17 μm. Then the laser power at the focal point was about 3×10^{10} W/cm^2. This was enough to

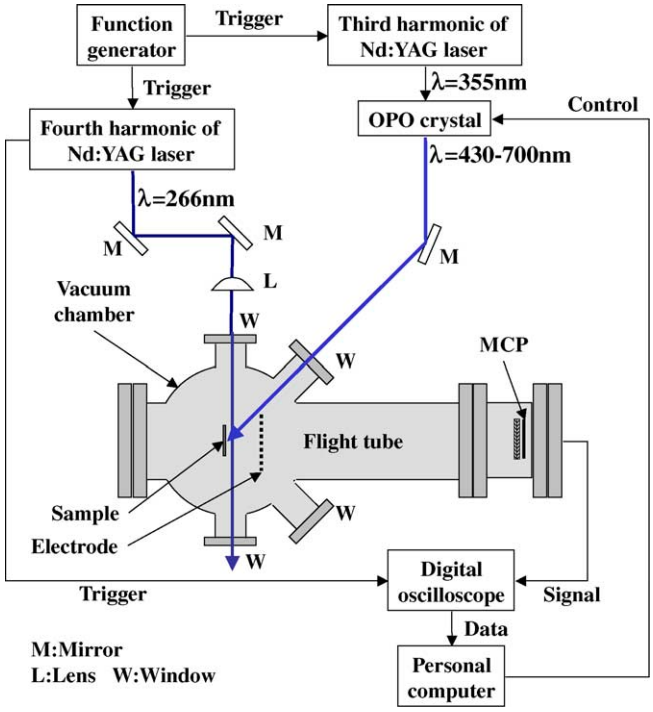

Fig. 1. Schematic diagram of the experimental arrangement for velocity distribution analysis of the desorption species by the laser irradiation.

ionize the gas by a multi-photon absorption process [9]. The delay time between the laser for desorption and that for ionization was controlled from 0 to 100 μs using a function generator. The distance between the sample and the laser for ionization was constant. The velocity of the desorbed species was evaluated using the delay time and the distance between the sample and the laser for ionization.

The ions generated from the desorbed neutral species by the laser irradiation for ionization were accelerated to an electrode at the ground by biasing the sample at a positive voltage (1000 V), and then detected by the MCP assembly. The distance between the electrode and the MCP was about 400 mm. The MCP signals were stored as a TOF spectrum in a digital oscilloscope and subsequently averaged.

Fig. 2 shows a signal of the residual water vapor ($M/e = 18$) in the chamber as a function of the laser power for ionization. This signal was well-fitted with $y = Ax^2$. The solid line in Fig. 2 is fitting result. This indicates that the ionization mechanism of water vapor using the laser for ionization is two-photon absorption process.

A plate of pure iron (99.9%, length: 40 mm, width: 10 mm, thickness: 0.5 mm) was used as a specimen in the present study. Electrolytic polishing was conducted using phosphoric acid for 10 minutes, and the plate was heated at 673 K in O_2 (20 Pa) for one hour to oxidize the sample surface. Thickness of the iron oxide layer was about several hundredths of a nanometer. From XRD analysis, it was found that the iron oxide layer was mainly Fe_2O_3. The sample surface was directly exposed to liquid D_2O in air for three hours at room temperature and lightly wiped with paper. Then the sample was placed in the vacuum chamber for TOF experiments. After the chamber was evacuated to about 10^{-4} Pa, the sample was irradiated with the laser for desorption. In this study, lasers at $\lambda = 355$ (3.5), 430 (2.9), 450 (2.8), 550 (2.3), and 600 nm (2.0 eV) were used for desorption. The sample was kept at room temperature in all experiments. The power of the laser for ionization was about 45 mJ/pulse.

Fig. 3(a) shows the intensity of $M/e = 18$ by the laser irradiation at $\lambda = 430$ nm (2.5 mJ/cm^2) as a function of the delay time between the laser for desorption and the laser for ionization. The distance between the sample and the laser for ionization was 3 and 4 mm. Fig. 3(b) shows the velocity distributions of the water which are transformed from the intensity shown in Fig. 3(a) using the distance between the sample and the laser for ionization. The peak position and the spread of the velocity distributions are almost same. This confirmed that the experimental results measured using this apparatus were appropriate. The experimental results which will be shown in the following session were obtained at a distance of 4 mm, because denser data could be obtained specially in the high velocity region.

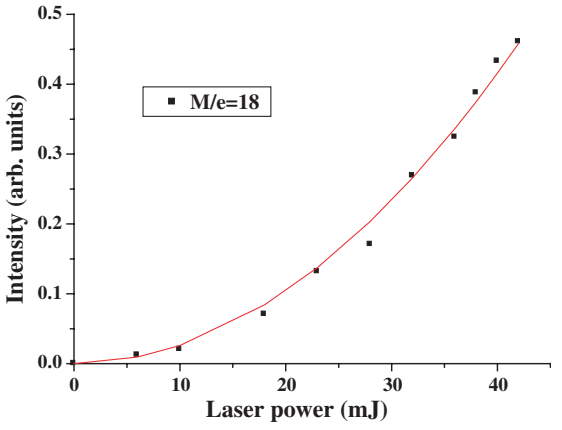

Fig. 2. A signal of the residual water vapor ($M/e = 18$) in the chamber as a function of the laser power for ionization.

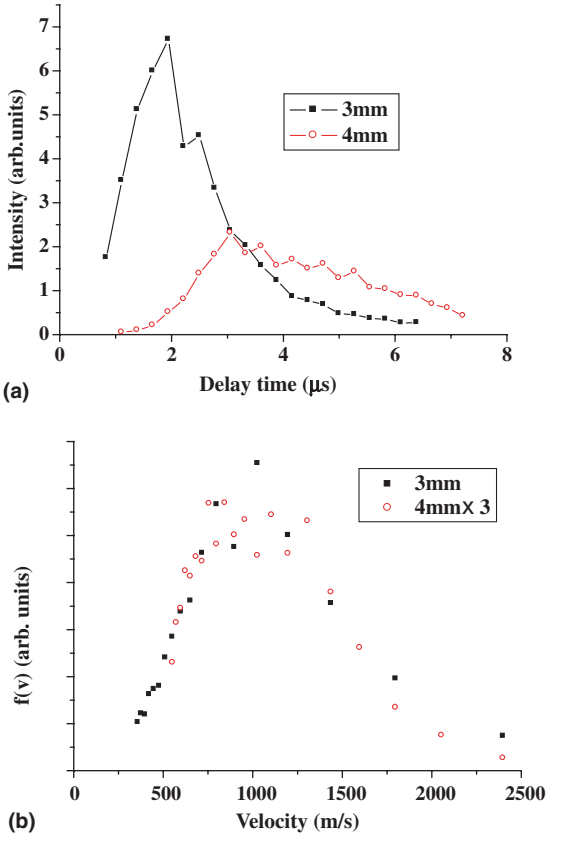

Fig. 3. Intensity of $M/e = 18$ as a function of the delay time between the laser for desorption and the laser for ionization (a) and velocity distribution (b) for the distance between the sample and the laser for ionization = 3 mm and 4 mm, and the laser for desorption at $\lambda = 430$ nm (2.5 mJ/cm^2).

3. Results

3.1. Mass analysis

MCP signals as a function of the flight time are shown in Fig. 4. When the laser for ionization was used without the laser for desorption (Fig. 4(a)), the residual gas in the vacuum chamber (10^{-4} Pa) was ionized. M/e = 1, 2, 12, 13, 14, 15, 16, 17, 18, 19, and 24 were the main species. However, when the residual gas in the chamber was detected using QMS, the main gas was water vapor. Therefore, M/e = 12, and 24 are considered to be generated by the ionization process using the laser at 266 nm from the carbon deposited on the inside of the chamber, and M/e = 1, 13, 14, 15 and 16 from the hydrocarbon gas in the chamber, given that hydrocarbons absorb a photon at λ = 266 nm and are decomposed. Since the signals of M/e = 12 and 24 linearly depend on the laser power for ionization, these are generated by single photon absorption. On the other hand, in order to ionize water vapor, two photons are required as explained above. Therefore, M/e = 12, and 24 generated from carbon by the ionization process using the laser at 266 nm are more sensitive than water vapor.

A MCP signal after the laser irradiation for desorption at λ = 430 nm is shown in Fig. 4(b). After the laser irradiation at λ = 430 nm, mainly M/e = 1, 2, 12, 13, 14, 15, 16, 17, 18, 19, 20 and 24 were increased. M/e = 2, 17, 18, 19, and 20 are considered to be hydrogen molecule or water. M/e = 12, and 24 are considered to be generated by the ionization process from carbon desorbed from the sample surface, and M/e = 1, 13, 14, 15 and 16 from the hydrocarbon desorbed from the sample surface. When the desorbed species by the laser irradiation for desorption at λ = 430 nm was detected using QMS, the main species was water. Since hydrocarbon gas or carbon is more sensitive than water vapor, as mentioned above, M/e = 1, 12, 24 are observed at TOF spectra clearly. Therefore, M/e = 2, 17, 18, 19, and 20 were analyzed. The results are reported below.

3.2. Energy threshold of the desorption

By TOF, the signals for M/e = 2, 17(OH), 18(H_2O or OD), 19(HDO), and 20(D_2O) were observed to occur by laser irradiation for desorption at λ = 355, 430, 450, 490 and 550 nm. But no signals were observed by laser irradiation at λ = 600 nm. These findings imply that there is an energy threshold around 550–600 nm (2.0–2.3 eV) for the desorption of these species. This threshold value roughly corresponds to the bandgap of Fe_2O_3 (2.2 eV). This suggests that desorption by the laser irradiation is initiated by the electronic excitation of the iron oxide.

Fig. 5 shows the intensity of M/e = 2, 17, 18, 19, and 20 by the laser irradiation at λ = 430 nm (2.5 mJ/cm^2) as a function of the delay time between the laser for desorption and the laser for ionization. The spectrum of M/e = 2 have two peaks. The time of the first peak (about 3 μs) was similar to that of the desorbed water. This indicates that this peak of M/e = 2 (D or H_2) is generated by the ionization process from the desorbed water. The second peak (about 5 μs) was considered to be generated by the ionization process from the heavier species than water such as hydrocarbon. If hydrogen molecule is desorbed from the surface by the laser irradiation for desorption, the velocity is higher than that of the desorbed water because hydrogen molecule is lighter than water. Then, the peak position of the hydrogen molecule would be shorter time than that of water. Consequently, it was considered that hydrogen molecule was not desorbed by the laser irradiation for desorption.

3.3. Dependence on the wavelength of the laser for desorption

The spectrum of M/e = 18 was mainly used for analysis in the present study for two reasons: one, as mentioned in the previous section, the desorbed species was water; two, the signal of M/e = 18 was largest. Fig. 6 shows the intensity of the desorbed M/e = 18 by laser irradiation at λ = 355, 430, and 450 nm (2.5 mJ/cm^2),

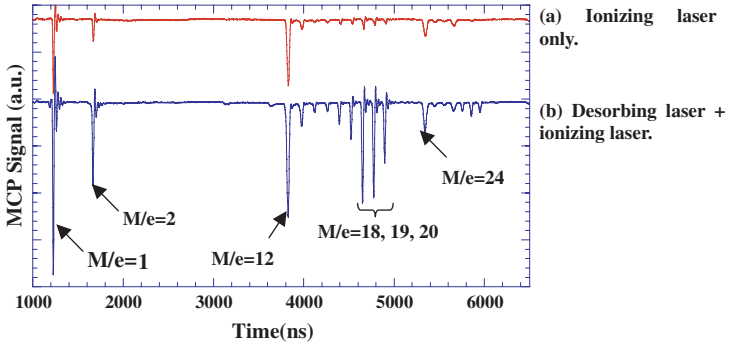

Fig. 4. TOF spectra: (a) ionizing laser only, (b) desorbing laser (430 nm, 2.5 mJ/cm^2) + ionizing laser (delay time: 3.3 μs).

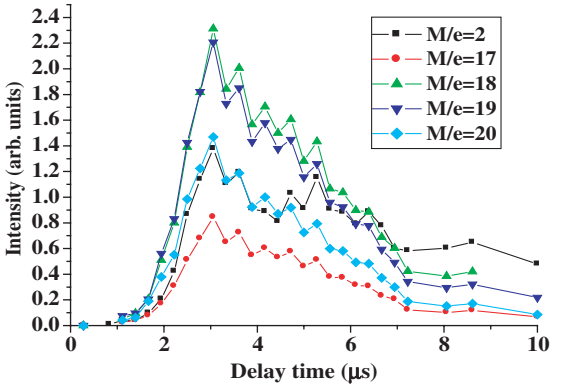

Fig. 5. Intensity of $M/e = 2$, 17, 18, 19 and 20 by the laser irradiation at $\lambda = 430$ nm (2.5 mJ/cm^2) as a function of the delay time between the laser for desorption and the laser for ionization.

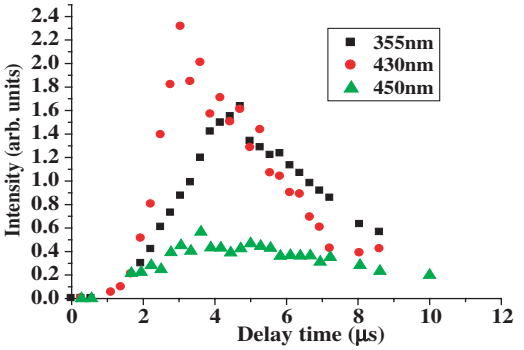

Fig. 6. Intensity of $M/e = 18$ by the laser irradiation at $\lambda = 355$, 430 and 450 nm (2.5 mJ/cm^2) as a function of the delay time.

respectively, as a function of the delay time. The spectra by laser irradiations at $\lambda = 355$ and 430 nm exhibited peaks at flight times around 5 μs and 3 μs, respectively. The peak by the laser irradiation at $\lambda = 430$ nm is clearly different from that at $\lambda = 355$ nm. This implies that the desorption mechanism is different between laser irradiation at $\lambda = 355$ nm and that at $\lambda = 430$ nm. The shape of the spectrum by the laser irradiation at $\lambda = 450$ nm was broad compared with the other two spectra, and its intensity was smaller than those of the other two.

3.4. Dependence on laser power

Fig. 7 shows the desorption yields of $M/e = 18$ as a function of the laser power at $\lambda = 355$, 430, and 450 nm. At $\lambda = 355$ nm, the desorption yield was well-fitted with an exponential function. The solid curve in Fig. 7 is fitting result. This suggests that the desorption is caused by a thermal process, because the desorption yield by the thermal process exponentially depends on

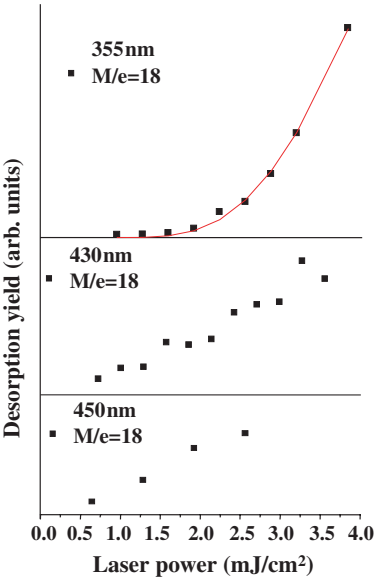

Fig. 7. The desorption yield of $M/e = 18$ as a function of the laser power at $\lambda = 355$, 430 and 450 nm.

the temperature, which is proportional to the laser power. On the other hand, by laser irradiation at $\lambda = 430$ or 450 nm, the desorption yield linearly depended on the laser power. This suggests that the desorption is caused by a single photon process and not by the thermal process.

3.5. Velocity distribution

Fig. 8 shows the velocity distributions of the desorbed water by laser irradiation at $\lambda = 355$, 430, and 450 nm. These velocity distributions $f(v)$ were transformed [10,18] from the observed intensity $I(t)$ as a function of the delay time by

$$f(v) = I(t)|\mathrm{d}t/\mathrm{d}v|v. \tag{1}$$

If the desorption is caused by the thermal process, the velocity distribution becomes the Maxwell–Boltzmann distribution

$$f(v) = Av^2 \exp(-Bv^2), \tag{2}$$

where A is the normalization factor and B the width parameter. B is related to the temperature by $B = m/2kT$, where m is the mass and k Boltzmann's constant. However, if the desorption is caused by the nonthermal process, the velocity distribution deviates from the Maxwell–Boltzmann distribution. In previous studies [10,12,13,16,17] of photon stimulated desorption, the velocity distribution of species desorbed by the nonthermal process under photon irradiation has been well-fitted with the 'modified' Maxwell–Boltzmann distribution [10,18]

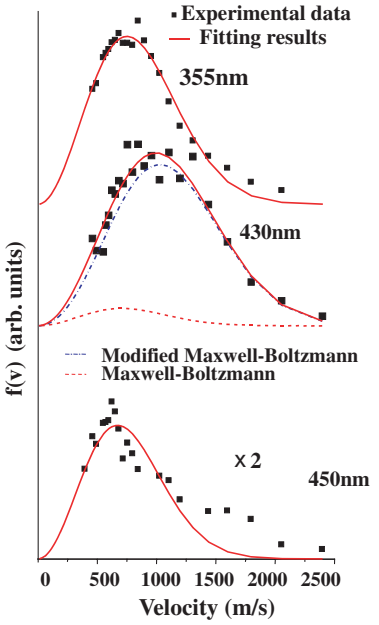

Fig. 8. The velocity distribution of the desorbed water by the laser irradiation at $\lambda = 355$, 430 and 450 nm (2.5 mJ/cm^2).

$$f(v) = Cv^2 \exp(-D(v - v_0)^2), \tag{3}$$

where C is the normalization factor, D the width parameter, and v_0 the flow velocity. This functional form was used for representing the velocity distribution of the particles desorbed from the surface by obtaining the kinetic energy via the nonthermal process [10,12,13,16,17]. The spread of the distribution was adjusted using the parameters D and v_0. If $v_0 = 0$, Eq. (3) is the pure Maxwell–Boltzmann distribution. Mean translational energy ($\langle E_{\text{trans}} \rangle$) is derived from the fitted curve by numerical integration [10,18], using the equation

$$\langle E_{\text{trans}} \rangle = \frac{1}{2} m v^2 = \frac{1}{2} m \frac{\int_0^\infty v^2 f(v) \mathrm{d}v}{\int_0^\infty f(v) \mathrm{d}v}. \tag{4}$$

The solid curves in Fig. 8 are the fitting results. The velocity distribution of water by laser irradiation at $\lambda = 355$ nm was well-fitted with a pure Maxwell–Boltzmann distribution, and the temperature inferred from fitting results was 610 K. It is considered that the desorption by laser irradiation at $\lambda = 355$ nm is mainly caused by the thermal process. However, in the high velocity region of the velocity distribution by laser irradiation at $\lambda = 355$ nm, the fitting results deviated from the experimental data. This means that desorbed water is the result not only of the thermal process but also of other processes, as will be mentioned below. The velocity distribution by laser irradiation at $\lambda = 430$ nm was fitted with the sum of a modified Maxwell–Boltzmann distribution and a Maxwell–Boltzmann distribution. The desorption by laser irradiation at $\lambda = 430$ nm is the result of the nonthermal process and the thermal process. From the fitting results, the majority of the desorbed water was considered to be the result of the nonthermal process. The temperatures of the thermal process and the nonthermal process inferred from the fitting result were 540 K and 790 K, respectively. The temperature of the nonthermal process was higher than that of the thermal process. In the case at $\lambda = 450$ nm, because the desorption yield was small, the distribution could not be fitted well using the sum of two distributions. In Fig. 8, the fit with Maxwell–Boltzmann distribution is shown. The temperature inferred from the fitting result was 490 K. The fitting result deviated from the distribution, especially in the high velocity region. Therefore, it is considered that the desorption by laser irradiation at $\lambda = 450$ nm is the result of the thermal process and the nonthermal process. Since similar results with several experiments were obtained, these dependence on the wavelength of the laser for desorption were considered to be valid.

As mentioned above, both thermal and nonthermal processes caused the desorption of water by laser irradiation at $\lambda = 355$, 430, and 450 nm. However, the amount of desorbed water was dependent on the wavelength of the laser. The amount of the water desorbed by the thermal process was large at $\lambda = 355$ nm, because the temperature evaluated from the fitting results using a Maxwell–Boltzmann distribution was higher at $\lambda = 355$ nm than at $\lambda = 430$ or 450 nm: 610 K at $\lambda = 355$ nm, 540 K at $\lambda = 430$ nm, and 490 K at $\lambda = 450$ nm. It is considered that the iron oxide on the surface absorbs the photons more effectively at $\lambda = 355$ nm than at $\lambda = 430$ or 450 nm, as will mentioned in Section 4. Therefore, the desorption yield of water by the thermal process at $\lambda = 355$ nm was large. On the other hand, the amount of water desorbed by the nonthermal process at $\lambda = 430$ nm was larger than that at $\lambda = 355$ or 450 nm. These findings will be discussed below.

4. Discussion

The desorption processes observed in these experiments were the result of the thermal process and the nonthermal process. Evidence that the nonthermal process is induced by laser irradiation is as follows:

(1) Intensity of the desorption signal of water is linear with the laser power at $\lambda = 430$ and 450 nm.
(2) The velocity distribution of the desorbed water by laser irradiation at $\lambda = 430$ or 450 nm did not become a Maxwell–Boltzmann distribution.
(3) The temperature of water inferred from the fitting results using the 'modified Maxwell–Boltzmann' distribution was higher than that of the thermal process.

The linear dependence of the desorption yield on the laser power indicates that the desorption process originates from a single photon process. In our previous study [5] using UPS spectra, water was dissociatively adsorbed on the sample surface and hydroxyls were formed. The binding energies of 1π and 3σ electrons of these hydroxyls were about 7 and 10 eV, respectively. Therefore, a single photon of the laser used for desorption in these experiments cannot directly excite the electrons of hydroxyls on the sample surface. This indicates that the initial process of the desorption is not electronic excitation of the hydroxyl adsorbed on the sample. The observed threshold of 2.0–2.3 eV corresponds to the bandgap of Fe_2O_3 (2.2 eV). UPS spectra and the energy threshold of the desorption imply that electronic excitation from the valence band to the conduction band in the iron oxide is the initial process for the desorption of water.

It is considered that some of these excited electrons in the iron oxide are scattered and de-excited, and the energy of these excited electrons is converted to heat on the sample surface. This conversion causes water desorption via the thermal process. The probability of electronic excitation of the iron oxide from the valence band to the conduction band by means of photon absorption is considered to become high with photons of higher energy, such as those used in this study. Consequently, the probability of electronic excitation by laser irradiation at $\lambda = 355$ nm is higher than that at $\lambda = 430$ or 450 nm and the temperature rise of the surface by the laser irradiation at 355 nm is larger than that at 430 or 450 nm. Therefore, the amount of water desorbed by the thermal process following laser irradiation at $\lambda = 355$ nm is larger than that at $\lambda = 430$ or 450 nm.

The electrons near the surface in the iron oxide those are excited by the laser irradiation are considered to promote the desorption of water by the nonthermal process. The excited electrons are considered to have been captured by the hydroxyls, after which the negative ionic state is generated on the surface. This formation of the ionic state promotes nonthermal desorption [12,13,17]. The electron transfer of the excited electron to the OH adsorbed on the surface is dependent on the energy of the OH orbital and the energy distribution of the exited electron. The energy distribution of the excited electrons is dependent on the energy of the incident photons. If the energy distribution is similar to the energy of 4σ empty orbital in OH adsorbed on the surface, the energy transfer of the excited electron to the adsorbed OH could efficiently occur. In the case of $\lambda = 430$ nm, the overlap between the energy distribution of the excited electrons and the energy of 4σ orbital of the OH adsorbed on the surface is considered to be large, leading to the efficient transfer of the excited electron to the OH, after which the negative ionic state is generated. Therefore, the desorption yield caused by the nonthermal process under the laser irradiation at $\lambda = 430$ nm is considered to be larger than that at $\lambda = 355$ or 450 nm. The electronic structure and the electron transfer system are schematically shown in Fig. 9. Since the photon penetration depth is on the order of 10^{-8} to 10^{-7} m, most of the electrons in the iron oxide that are excited by the laser irradiation will not reach the surface and interact with an adsorbed species before being subject to scattering or de-excitation [9]. This is because the lifetime of excited electron is short, on the scale from 10^{-15} to 10^{-13} s, and a typical velocity of the electron is of order 10^6 m/s. Therefore, most of the electrons excited in the iron oxide are considered to be scattered and de-excited, and only the excited electrons near the surface are transferred to the surface hydroxyls and cause the nonthermal process. The number of the excited electrons that contribute to the nonthermal process is considered to be small.

The desorption via a negative ionic state like that generated by the process mentioned above follows the change of the potential energy surface between the surface and OH [13,17]. The excitation via the electron transfer from the surface to OH is a Franck–Condon transition to a negative ionic state. The negative ionic state has an equilibrium position that is closer to the surface than that of the ground state, because the OH is charged in plus and the surface in minus. Following the electron transfer, the OH on the negative ionic state is attracted to the surface. After lifetime of the excitation state, the OH on the negative ionic state de-excites to the ground state via electron returning to the surface. This de-excitation process is again a Franck–Condon transition. On the negative ionic state, the OH gains the kinetic energy. The kinetic energy depends on the lifetime of the negative ionic state. After de-excitation, the OH is repelled from the surface on the ground state. The lifetime of the excited state is considered to lie between 10^{-15} and 10^{-13} s [9]. The lifetime is considered

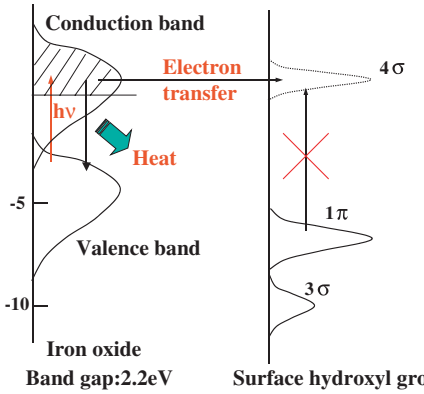

Fig. 9. The electronic structure of the iron oxide valence band and conduction band, and that of OH adsorbed on the surface.

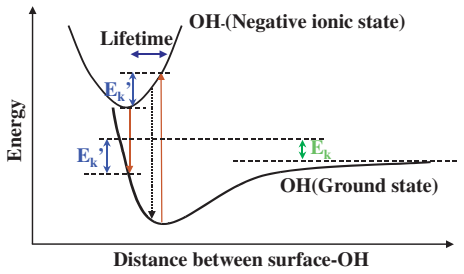

Fig. 10. Schematic potential energy surface for water desorption from the sample surface [10].

shorter than the time of a vibration between the surface and the hydroxyl on the negative ionic state (about 10^{-13} s). If the time of de-excitation from the negative ionic state to the ground state is long, the kinetic energy gained by the negative ionic state is enough to overcome the binding energy and the bonding between the OH and the surface is cut. In Ref. [13], O–H bonding of OH which captures the electron is cut and the H atom gains the energy. This H atom reacts with the neighboring OH and H_2O is desorbed. However, in the present study, the bonding between the OH and the surface is considered to be cut. This is because in our previous study [5], O–H bonding was cut by the irradiation of the photon with the energy higher than about 10 eV and the hydrogen molecule (H_2) was detected. In the present study, no hydrogen molecule was detected. Therefore, the bonding between the OH and the surface is cut. On the other hand, if the time of de-excitation from the negative ionic state to the ground state is short, the kinetic energy is not enough to overcome the binding energy. This mechanism is schematically shown in Fig. 10. The time from the capture of the excited electron to the desorption is estimated to be about 10^{-13} s from the time scale of a vibration between the surface and the hydroxyl. Since about 10^{-12} s is necessary to equilibrium with the surface, the desorption water is not in equilibrium with the surface. Therefore the velocity distribution did not become a Maxwell–Boltzmann distribution and the temperature is high. It is considered that the desorbed OH reacts with the neighboring OH and water desorbed, since this desorbed OH is reactive.

5. Conclusions

The following mechanisms of desorption of water from an iron oxide by UV-visible laser irradiation were considered based on the results of the TOF experiments:

(1) The desorption of water adsorbed on the iron oxide surface is initiated by the electronic excitation in the iron oxide from the valence band to the conduction band.
(2) The majority of the energy of the excited electrons in the iron oxide is considered to be converted to heat on the sample surface, and this temperature rise is considered to cause the desorption of water via the thermal process.
(3) In the nonthermal process, the electrons in the iron oxide exited by the laser irradiation were considered to be transferred to the surface hydroxyls, where they generate a negative ionic state on the surface. The negative ionic hydroxyls caused the water desorption. The amount of water desorbed by the nonthermal process had a peak at around $\lambda = 430$ nm.

References

[1] N. Masaki, T. Hirabayashi, M. Saeki, Fus. Technol. 15 (1989) 1337.
[2] J.P. Krasznai, R. Mowat, Fus. Technol. 28 (1995) 1336.
[3] Y. Oya, T. Tadokoro, W. Shu, T. Hayashi, S. O'hira, M. Nishi, J. Nucl. Sci. Technol. 38 (2001) 967.
[4] K. Chiba, T. Yoneoka, S. Tanaka, Fus. Technol. 39 (2001) 1038.
[5] K. Chiba, R. Sato, T. Yoneoka, S. Tanaka, Fus. Sci. Technol. 41 (2002) 386.
[6] K. Chiba, R. Sato, T. Yoneoka, S. Tanaka, Fus. Eng. Des. 61&62 (2002) 775.
[7] K. Chiba, R. Ohmori, T. Yoneoka, S. Tanaka, Phys. Scr. T 103 (2003) 125.
[8] T.J. Chuang, Surf. Sci. Rep. 3 (1983) 1.
[9] X.-L. Zhou, X.-Y. Zhu, J.M. White, Surf. Sci. Rep. 13 (1991) 73.
[10] F.M. Zimmermann, W. Ho, Surf. Sci. Rep. 22 (1995) 127.
[11] M. Wolf, S. Nettesheim, J.M. White, E. Hasselbrink, G. Ertl, J. Chem. Phys. 92 (1990) 1509.
[12] M. Wolf, S. Nettesheim, J.M. White, E. Hasselbrink, G. Ertl, J. Chem. Phys. 94 (1991) 4609.
[13] X.-Y. Zhu, J.M. White, M. Wolf, E. Hasselbrink, G. Ertl, J. Phys. Chem. 95 (1991) 8393.
[14] S. Ferrer, G.A. Somorjai, J. Phys. Chem. 85 (1981) 1464.
[15] C.L. Perkins, M.A. Henderson, J. Phys. Chem. B 105 (2001) 3856.
[16] K. Fukutani, A. Peremans, K. Mase, Y. Murata, Surf. Sci. 283 (1993) 158.
[17] K. Fukutani, Y. Murata, R. Schwarzwald, T.J. Chung, Surf. Sci. 311 (1994) 247.
[18] F. Budde, T. Gritsch, A. Modl, T.J. Chuang, G. Ertl, Surf. Sci. 178 (1986) 798.